Modulus and Chemical Mapping of Multilayer Coatings

Aaron M. Forster,*,† Chris A. Michaels,‡ Lipiin Sung,† and Justin Lucas†

National Institute of Standards and Technology, Gaithersburg, Maryland 20899-8615

ABSTRACT Thermoplastic olefins (TPOs) are polymeric materials utilized for interior and exterior automotive parts. These materials are often painted to protect and enhance their appearance. TPO materials possess a low surface energy because of the aliphatic backbone, and adhesion promoters (APs), such as chlorinated polyolefins, are used to increase paint adhesion and improve paint performance. The impact of the AP structure and processing conditions on the mechanical properties and degree of interpenetration was investigated on cross sectioned coatings. The AP structure was varied by the chlorine content and molecular weight for the same TPO and polyester acrylic, melamine-cured paint system. Two different processing conditions were investigated. Mechanical properties were measured using depth-sensing indentation. Long-range diffusion of coating components across each interface was verified with confocal Raman microscopy. The AP interfaces, AP/base coat and AP/TPO, were chemically and mechanically sharp at the 1 μm lateral resolution of both techniques. Depth-sensing indentation measured a modulus gradient across the top coating cross section. The free air surface of the top coat had a higher modulus than the interior. Processing conditions and polishing to prepare the cross section for measurements were found to affect only the control AP.

KEYWORDS: nanoindentation • polyester acrylic • melamine • modulus • thermoplastic polyolefin • confocal Raman microscopy • chlorinated polyolefin • adhesion promoter

INTRODUCTION

Thermoplastic olefin (TPO) is a semicrystalline polypropylene blended with a phase-separated ethylene–propylene or ethylene–butene rubber. Polypropylene is a brittle material that has a low impact strength but is suitable for processing into complicated shapes using injection-molding techniques. Pure polypropylene fails via the formation of crazes upon impact. The dispersed rubber phase improves the toughness of the polypropylene matrix by halting the propagation of crazes within the matrix. The advantages of TPO compared to steel include lower cost, extended durability, recycling of used parts, and the ability to form parts into complicated shapes and surface textures. TPO accounts for ≈60% of interior parts and ≈85% of exterior parts (1) for automotive applications. Despite these multiple advantages of TPO, there are two main shortcomings: the TPO microstructure is sensitive to processing conditions, and its low surface energy (2) makes it difficult for automotive coatings to bond to it. There have been several relevant research efforts to measure the TPO microstructure and methods to increase coating adhesion to TPO (2–5).

A conceptual view of the TPO microstructure is given in Figure 1a (6–8). The bulk TPO is composed of a dispersed rubber phase, with rubber particles having diameters between 1 and 20 μm, within the polypropylene matrix. The rubber phase morphology shifts from spherical to elliptical or fibril in a 2–3 μm region below the surface. At the near-surface is a polypropylene-rich layer with a shear-induced crystalline structure that can contain narrow fibrils of dispersed rubber depending on the rubber concentration within the TPO. This nonequilibrium morphology is due to shear flow from injection-mold processing and rapid cooling within the mold. Ryntz (9) has shown that processing variables such as the gate volume, injection speed, and mold temperature have a significant impact on the thickness and morphology of this near-surface region, and this microstructure is important when considering adhesion to TPO.

A common method used to improve adhesion is to spray-apply low-molar-mass chlorinated polyolefin adhesion promoters (APs). Although the specific mechanism of adhesion is currently not known, a general picture of the mechanism has emerged. The solvent in the AP solution penetrates and swells the buried rubber phase. This permits diffusion of the lower molecular weight aliphatic AP into the TPO, which provides mechanical interlocking and alters the TPO surface energy (1, 10, 11). In addition to solvent application, the AP layer and TPO are often baked at 120 °C to promote further diffusion between the materials. This higher temperature is significant because it is above the melting point of the impact modifier but below the melting point of the polypropylene matrix. Mirabella et al. (12) calculated the thermodynamic equilibrium thickness between a lower molecular weight polyolefin and TPO based on an estimated Flory–Huggins interaction parameter, χ. They estimated that the AP will penetrate the TPO to a depth of 11 nm at 25 °C. A separate calculation based on the diffusion coefficient of the lower molecular weight polyolefin into the TPO during application at 25 °C would be on the order of 10–20 coil diameters or

* E-mail: aaron.forster@nist.gov.

Received for review October 29, 2008 and accepted January 16, 2009

† Materials and Construction Research Division.

‡ Surface and Microanalysis Science Division.

DOI: 10.1021/am800152x

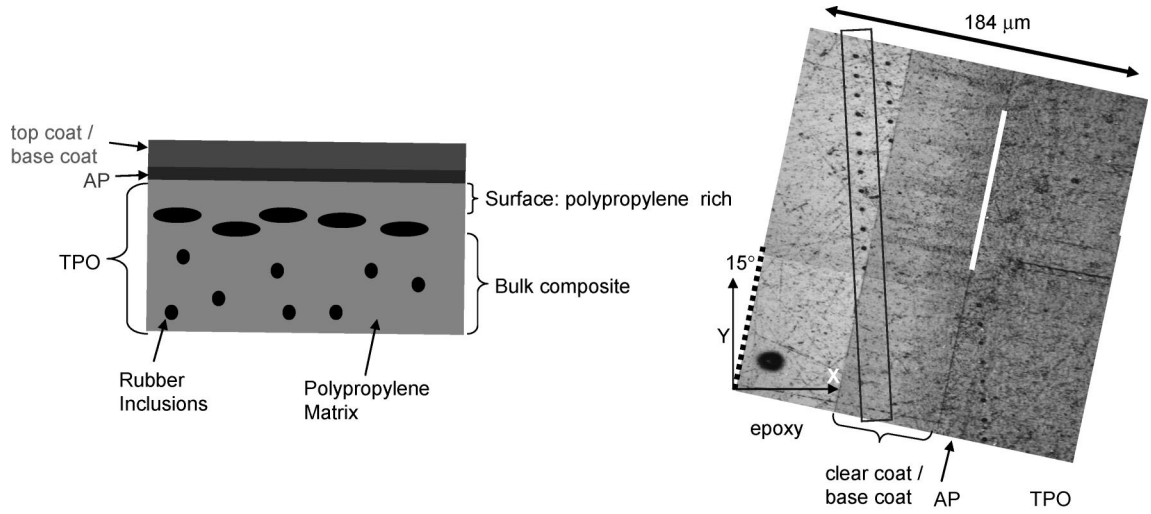

FIGURE 1. (a) Generalized view of the TPO microstructure and the laminate construction of a painted TPO (not to scale). (b) LSCM composite image (50×) of the laminate sample. The box highlights a line of indents through the laminate sample. Note the elastic recovery within the BC and TC regions. The epoxy is only used to mount the sample for polishing. The white line is a guide for the eye to the AP/BC interface.

200−400 nm. On the basis of diffusion alone during a 120 °C bake for 30 min, the depth would approach 5000 nm, although this was unlikely because of the limit established by thermodynamic equilibrium. Scanning transmission X-ray microscopy of AP-coated TPO samples, baked at 120 °C, showed a sharp interfacial thickness of approximately 350 nm (12). Tang and Martin conducted transmission electron microscopy imaging and interfacial adhesion studies of painted TPOs after the coating failed (13). They found that baking at high temperature in the presence of solvent increased the diffusion length of AP into the dispersed rubber phase of the TPO substrate. Ryntz and coauthors conducted several studies combining Raman imaging or confocal microscopy of TPO coated with an AP dissolved in a solvatochromatic dye (Nile red). The authors found that the tagged solvent penetrates up to 20 μm into the TPO substrate and preferentially into the rubbery regions (6, 7). An earlier study using time-of-flight secondary-ion mass spectrometry (TOF-SIMS) experiments found that the interface between the AP and TPO had a diffuse character, but the limits of instrument resolution did not permit a quantitative measurement (4). In other cases, solvents that were preferential to the dispersed rubber phase caused swelling of the rubber near the polypropylene surface and the rubber diffused into the AP layer up to 500 nm (8, 13). Ma et al. (8) investigated wiping of the TPO surface with solvents prior to painting with a fluorescently (benzothioxanthene) tagged AP. Confocal microscopy was used to characterize the buried TPO/AP interface width. Nonwiped TPO and wiped pure polypropylene substrates exhibited a sharp interface (<0.5 μm), while solvent-wiped TPO substrates exhibited a more diffuse interphase up to 2 μm thick. The observation of a diffuse interphase was tempered by profilometry measurements that showed that the roughness of the TPO substrates also increased after solvent wiping. Therefore, it was not conclusive whether the larger interphase width was due to an increase in the surface roughness or diffusion.

The TPO structure, top-coat toughness, AP diffusion, and AP structure have been shown to affect coating adhesion to TPO substrates. Ryntz et al. (14) used a compressive shear delamination test to highlight the complexity of the adhesion problem by demonstrating that the selection of a solvent and AP must take into account the toughness of the top coat and the strength of the TPO. More recently, adhesion research has focused on the TPO/AP interface. Yin et al. (15) used confocal microscopy of a fluorescently tagged AP to determine the locus of failure of TPO lap shear joints. The authors found that surface preparation of the TPO via solvent wiping leads to higher fracture energy and *cohesive failure* within the AP, compared to *adhesive failure* for the AP on a pure polypropylene surface. The local TPO structure was found to be important because local increases in the rubber concentration aided AP diffusion. The importance of the local AP structure was reinforced by Lawniczak et al. (3). Atomic force microscopy measurements were used to measure the local crystallinity and surface roughness in chlorinated and nonchlorinated APs. The authors found that increasing the crystallinity of the AP can increase the 90° and 180° peel strengths of top coats from TPO substrates.

The development of a unified model for AP diffusion is complicated because of the heterogeneous surface structure of the TPO. In general, it is agreed that solvent swelling and baking above room temperature improve coating adhesion by promoting diffusion and mechanical interlocking of the AP into the rubbery regions of the TPO, although the ultimate diffusion length scale is a function of the local TPO structure, AP structure, and solvent. The complexity of these systems and the potential for improvement in performance via a stronger interfacial bond drives the continued research into the interfacial region of automotive coatings using new analytical tools. The impact of the AP structure and processing on local mechanical properties has not received sufficient attention. AP diffusion lengths greater than a micrometer

would be expected to impact the mechanical properties of both the paint and the TPO substrate.

Depth-sensing indentation (DSI) has been an effective tool to measure the local modulus and hardness through the thickness of automotive coatings (16) and weathered coatings (17). In this work, we investigate the properties of the TPO, AP, and paint layers using a combination of DSI and confocal Raman microscopy. Confocal Raman microscopy is a nondestructive optical technique for generating surface compositional maps using the unique spectroscopic signatures of the various chemical constituents. This technique yields information comparable to that acquired from SIMS without complications due to ion-induced cross-linking within the specimen. A high lateral resolution can be achieved (<1 μm), and little sample preparation is required. The combination of techniques is intended to provide complimentary information on these multilayer systems. Several questions will be addressed: Will optical microscopy, chemical spectroscopy, and mechanical measurements yield similar information on whether the AP/TPO interface is greater than a micrometer? Does the AP structure alter the mechanical properties within the multilayer system? Does the processing method impact the mechanical properties or spectroscopic signature of any layer in the multilayer coating?

EXPERIMENTAL SECTION

The adhesion promoters (APs) were provided by Eastman Chemical (3). The TPO panel coupons contained 20 wt % rubber and a medium crystallinity. Painted samples were assembled at Visteon. The panels were coated with the AP primer, base coat (BC), and top coat (TC), and a graphic of the laminate structure is shown in Figure 1a. The dry layer thicknesses, as reported by Visteon, were as follows: BC, 35 μm; TC, 17 μm; AP, 7.5−10 μm. The dry layer thicknesses were measured via optical microscopy of cryomicrotomed cross sections. Two sets of painted samples were made: (1) unmounted coupons and (2) cross sectioned coupons that were mounted in epoxy and polished. Unmounted coupons of TPO/AP, TPO/AP/BC, and TPO/AP/BC/TC were made for comparison to the cross sectioned samples to determine whether polishing affected the mechanical properties. The cross sections were polished using a mechanical grinding process with successive grits of silicon carbide papers (320, 500, 800, 1200, and 4000) followed by a final polish using a 1 μm diamond-suspension polish.

Three different AP materials were investigated. The control promoter, designated CNTL, contained ≈22 mass % chlorine. A high chlorine promoter, designated Cl, contained 25 mass % chlorine but the same molecular weight as that of CNTL. The high molecular weight promoter, designated MW, contained the same molar mass of chlorine as that of CNTL but a higher molecular weight. The BC and TC chemistries were the same: a solvent-borne one-component polyester acrylic system cured with a melamine cross-linker. The BC layer contained no pigment to reduce fluorescence and scatter in the Raman measurements. Two methods were used to process the samples. The first method is the *wet-on-wet method* (WOW). In this method, the AP, BC, and TC are applied in succession. There is a short solvent flash time allowed between the application of each coat, and the painted part is placed in the oven to fully cure. For the WOW process, the AP, BC, and TC were spray-applied and the solvents allowed to flash evaporate between applications for periods of 3, 5, and 10 min, respectively. The coated part was baked at 120 °C for 30 min.

The second method is defined as the *bake method*, where the AP is applied to the TPO and baked at 120 °C for 30 min. The BC and TC were applied after the TPO was removed from the oven and cooled to room temperature. The flash time, final bake time, and temperature in the BC and TC application were the same as those in the WOW application. This experimental matrix provides three different APs subjected to two different processing conditions for a total of six separate samples.

DSI. Measurements were performed using a commercial nanoindenter (MTS Nanoinstruments, NanoXP). To achieve a higher resolution placement of the indents, the sample was mounted with the cross section at an angle to the *Y* axis that ranged between 10° and 15°; see Figure 1b. Indents were conducted in a vertical line (*Y*-axis motor only) progressing from the mounting epoxy toward the TPO. Spacing between indents was 15 μm, which translated to between 2.5 and 4 μm lateral movement (*X* direction) toward the TPO interface. Three lines of 60 indents (180 indents/sample) were used to create moduli and hardness maps. The absolute position of each indent and its relationship to each interface was measured using laser scanning confocal microscopy (LSCM). The lateral image pixel size is 0.37 μm, whereas the resolution is nominally 0.5 μm, as determined from the incident laser wavelength (543 nm) and the numerical aperture of the objective (0.5) (18). The AP/BC interface was used as the zero reference position because it was a well-defined and a readily locatable landmark. Drzal et al. (16, 17) used a similar procedure to investigate the moduli of coated TPO panels via DSI.

A 1 μm radius, 60° diamond cone indenter was used to indent the samples. Loading was performed at a constant strain rate of 0.05 s^{-1}. The harmonic contact stiffness of the tip/sample contact was continuously measured during indentation by imposing a small oscillation of 2 nm at a frequency of 45 Hz. Reported values of the modulus for each indent were averaged over a depth range from 500 to 1000 nm without a drift correction. The maximum contact radius was ≈1 μm for an indentation strain of 20%, and the measured modulus was constant within this depth range. Poisson's ratio was assumed constant and equal to 0.35. Several references are available to utilize load, displacement, and stiffness data to determine the modulus and hardness (19−23), although these are not discussed in detail here.

DSI utilizes an axisymmetric probe tip to indent a material, at a controlled loading rate, to a prescribed maximum load or displacement. For elastic−plastic deformation, the initial unloading of the tip from the maximum load is elastic. Oliver and Pharr (21) employed Hertzian contact mechanics to calculate the elastic contact stiffness, *S*, from the slope of the initial or elastic portion of the unloading curve. *S* is the change in the load with displacement or d*P*/d*h*, where *P* is the load and *h* is the displacement. This contact stiffness, *S*, is used with eq 1 to determine the reduced elastic modulus, E^*, for a circular contact area.

$$E^* = \frac{\sqrt{\pi}}{2\sqrt{A}} S \tag{1}$$

$$\frac{1}{E^*} = \frac{\left(1 - \nu_i^2\right)}{E_i} + \frac{\left(1 - \nu_s^2\right)}{E_s} \tag{2}$$

where A is the contact area, E_i is the modulus of the indenter, E_s is the modulus of the sample, ν_i is the indenter's Poisson ratio, and ν_s is the sample's Poisson ratio. The hardness is defined as the mean stress beneath the indenter (eq 3).

$$H = P/A \tag{3}$$

where P is the load and A is the contact area. A variation in indentation is dynamic indentation or continuous stiffness

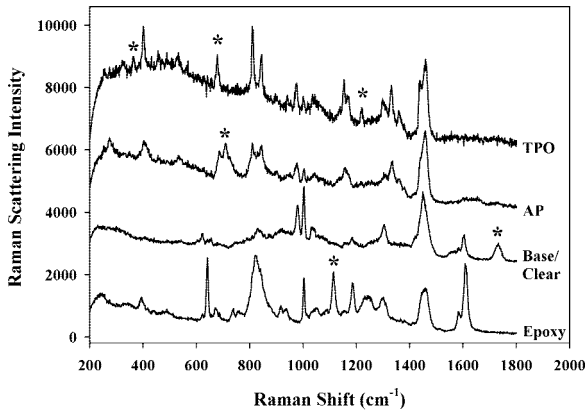

FIGURE 2. 785 nm Raman spectra of the pure coating system materials. Selection of the chemical specific marker bands (*) used in the generation of line-scan component maps is provided in the text. Each spectra is offset vertically for visual clarity.

measurement. In this case, a small oscillation is superimposed over the tip loading profile. The tip/sample interaction and machine contribution are modeled using a series of springs and dashpots (damped harmonic oscillator) to measure the elastic component of the contact stiffness, S (21), during loading. Because each oscillation provides a measure of the contact stiffness, the elastic modulus and hardness are measured as a function of the depth during indentation. Other advantages include better sensitivity to the surface and the ability to better separate the elastic contribution of a viscoelastic material.

Confocal Raman Microscopy. Details of the confocal Raman microscope used to evaluate the cross sectioned samples are described elsewhere (24). The analysis of these samples with confocal Raman is similar, in some respects, to that of Adamsons, which produced depth-profile measurements of the chemistry of weathered automotive coatings via IR and UV−vis measurements (25). Mapping of the various layers present in the multilayer sample requires identification of marker Raman bands for each species extracted from spectra of the pure materials. These bands are chosen on the basis of their specificity for the material (i.e., minimal overlap with spectral features of other proximate species) and their intensity. Characteristic Raman spectra of the four layers present in the multilayer sample—TPO, AP, BC, TC—and the mounting epoxy are shown in Figure 2. These spectra are offset vertically for visual clarity, and the marker bands discussed below are indicated by asterisks. The variation in the noise levels in these spectra is due to the shot noise on the varying levels of background fluorescence seen in each spectrum.

The methylene torsion band of polypropylene at 1220 cm^{-1} was chosen for mapping of the TPO layer (26) because this relatively weak band shows little overlap with the AP spectrum. (Note that this band shows significant overlap with a band in the epoxy spectrum. This does not present any difficulty because these layers are separated by the AP and BC/TC layers.) The presence of talc complicates the mapping results for the TPO layer. Regions of high talc concentration (talc can be mapped using the 366 or 679 cm^{-1} band (27)) yielded smaller levels of polypropylene, leading to large apparent concentration fluctuations in the maps of the TPO region. This complication is difficult to avoid given that the compositional heterogeneity of the TPO exists over length scales larger than the microscope resolution. The variations seen in the mapping on the TPO region are largely a reflection of a change in the local concentration of talc. The C−Cl stretching bands in the 660−730 cm^{-1} region were chosen as the marker bands for the AP. This spectral feature is the main band that distinguishes the AP from TPO and thus is the only realistic choice for this species. The band area in this case was calculated by integration over the high-frequency half of the peak and doubling of this area. This was done to avoid interference with a strong Si−O−Si talc band at 679 cm^{-1}. The clear BC and TC layers were indistinguishable because the pigment was removed from the BC to avoid compromising the index matching between the immersion oil and the sample. The carbonyl band at 1730 cm^{-1} was chosen as the marker band for these two indistinguishable layers. Finally, the 1116 cm^{-1} band, presumably an oxirane wag vibration, is used to map the mounting epoxy.

Certain instruments or materials are identified in this paper in order to adequately specify experimental details. In no case does it imply recommendation or endorsement by NIST or imply that it is necessarily the best product for the experimental procedure.

RESULTS AND DISCUSSION

Figure 3 is a representative Raman line-scan map of a laminate containing the MW AP fabricated using the bake method (2a) and the WOW (2b) method. Because the results for both methods are similar, the baked sample will be highlighted in the following discussion. The band area values at each point in the line scan are normalized to the maximum value for that band to enable a comparison between species. In the range 0−10 μm, the predominant species is TPO, although the AP, BC, and TC bands show nonzero values. Further inspection of the spectra in this region reveals that this nonzero value is due to minor spectral overlap with the TPO marker band and is not due to the presence of the BC or AP in the TPO region. The large variation in the TPO band area in this range is largely due to variation in the talc concentration and is reflective of the heterogeneity of TPO as opposed to measurement noise. The sharp TPO/AP interface can be seen clearly at about $x = 12$ μm, where the AP value quickly increases to a near-maximum value and the TPO band area drops to a lower level. The TPO value in the AP region is again due to the minor presence of spectral intensity in the AP spectrum within the TPO marker band region. This is not surprising given the chemical similarity between the AP and polypropylene. These complications aside, the important observation is that this interface is quite sharp, with a measured width of less than 1 μm, a value that is certainly limited by the instrument resolution. There is also no evidence of large-scale diffusion of AP into the TPO layer at the micrometer length scale, although it is important to note that diffusion at levels below a few percent would likely fall below the sensitivity of this measurement. The AP/BC interface is seen clearly at around $x = 20$ μm, where the C−Cl stretching band value quickly drops to near zero and the BC value rises rapidly to its maximum value. Again the interface sharpness appears to be instrument-limited (<1 μm), and there is no evidence of significant diffusion between these two layers. Finally, the interface between the clear coat and the mounting epoxy is apparent at $x = 63$ μm. Several other features of this map are noteworthy. The small peak in the TPO and AP profiles at $x = 31$ μm is due to a change in the slope of the fluorescence background in this region, which leads to a nonzero band intensity. This peak is purely an artifact of how this strongly shifted background influences the TPO and C−Cl band area calcula-

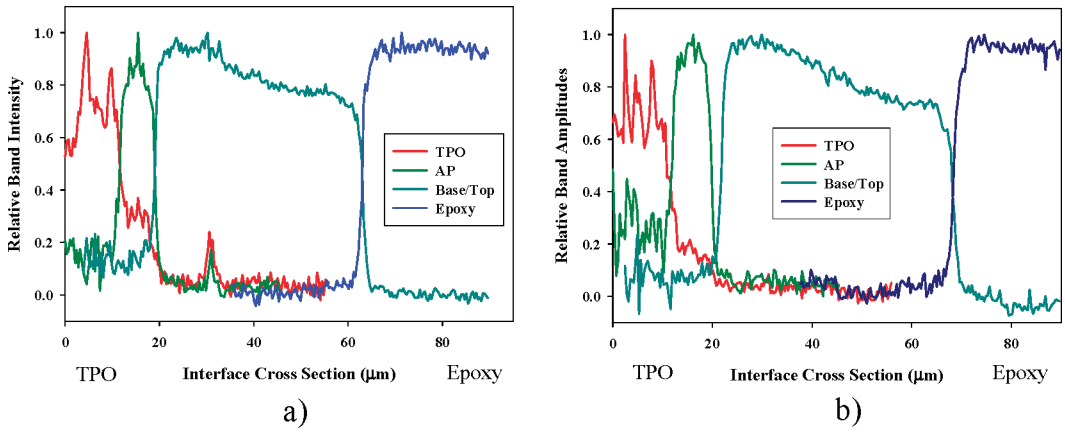

FIGURE 3. (a) Raman line-scan component maps of the polished MW bake sample cross section. The relative band intensity for each material is related to the intensity of the marker band defined in Figure 2. (b) Raman line-scan component maps of the polished MW WOW sample cross section. The relative band intensity for each material is related to the intensity of the marker band defined in Figure 2.

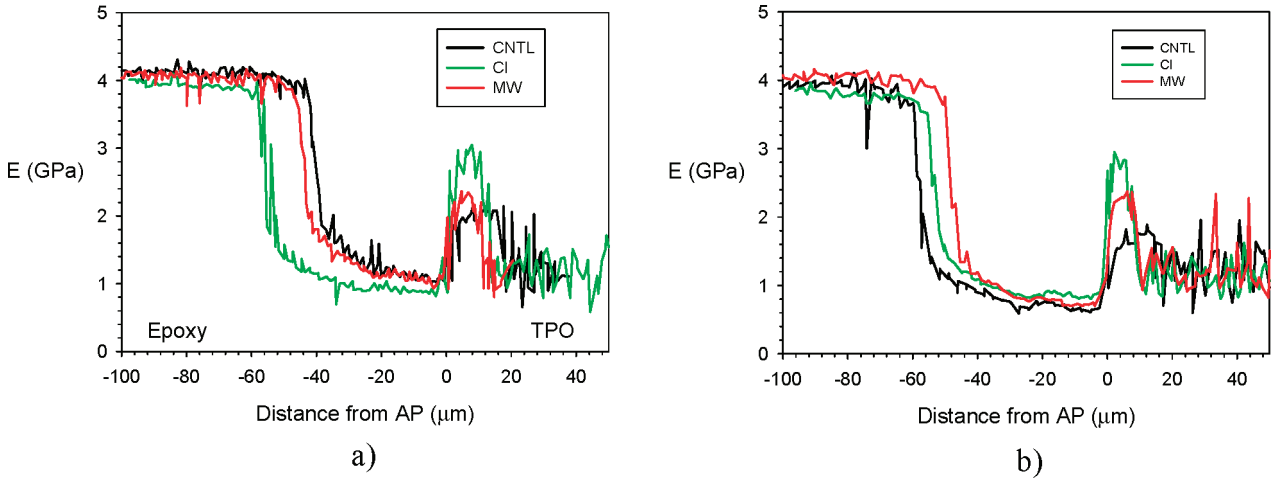

FIGURE 4. Moduli measured across the thickness of the polished laminate samples. Samples prepared with the (a) bake method and (b) WOW method. Zero is the BC/AP interface. The standard deviations in the modulus measurement were ±0.05 GPa within the BC/clear coat region and ±0.25 GPa within the TPO region.

tions. The origin of the changing fluorescence background is unknown but might well be due to some small surface contaminant. The slow decline in the band intensity across the BC/TC region is likely due to a small drift of the sample with respect to the laser focus (data acquisition across this region took approximately 4 h), slightly reducing the overlap between the laser and the sample.

Similar Raman line scans were recorded for all six samples (one other example of which can be seen in Figure 3b for the MW WOW sample) at several positions. In addition, a number of high-resolution 32-μm-width scans focused on the AP interfaces were also recorded. In each case, the results were essentially the same. The widths of the TPO/AP and AP/BC interfaces were measured to be nominally 1 μm, a value likely limited by the instrument resolution. Additionally, no evidence was found for significant diffusion of the AP into either the BC or TPO layer. These conclusions were independent of the AP structure and processing method.

Figure 4 shows indentation modulus measurements for the three different multilayer samples prepared with the bake and WOW processing, respectively. The AP interfaces are sharp, confirming little diffusion across the AP interfaces. Similar to Raman spectroscopy, the modulus within the TPO varies significantly. The width of the CNTL, Cl, and MW layer estimated from both indentation and Raman microscopy is approximately 8−10 μm, which is within the range of the dry layer thickness. It was not possible to quantitatively verify the width of any AP layer using only optical confocal microscopy because the AP/TPO interface lacks sufficient contrast. Ma et al. (28) have demonstrated a method to utilize fluorescently tagged AP materials to measure the concentration fluctuations, but that method was not employed here.

Indentation measurements show that processing had the greatest effect on the CNTL modulus. The modulus of WOW CNTL (E = 1.66 GPa) was 17% lower than the modulus of the baked CNTL (E = 2.01 GPa). The moduli of the Cl and MW AP did not change as a function of processing.

An advantage of DSI over traditional modulus measurement techniques is observed in the BC and TC layer in Figure 4. In both samples, the modulus of the TC increases as the indenter moves toward the epoxy/TC interface, which could not be measured using traditional bulk testing methodologies. Because the epoxy modulus is greater than the TC modulus, near this interface the epoxy may confine the

movement of the TC underneath the indenter and increase the measured contact stiffness. This would result in an increase of the TC modulus. A general estimate of the size of the stress field around the sphere for axisymmetric indentation, which could affect the modulus measurement on the TC, is 2 times the contact radius (29, 30). For this test geometry, indentations within 3 μm of an interface are within this zone. As seen in Figure 4, the modulus begins to increase $\approx$15 μm from the epoxy interface, significantly farther from the epoxy interface than was estimated from elastic contact mechanics. While the origin of the modulus increase is the subject of future work, we believe this originates during skin formation induced from the combination of solvent evaporation and paint cross-linking during the spray application process (31). Information about the modulus of the coating within the cross section as a function of the processing method is valuable for determining the impact of process changes on the surface modulus of coatings (32).

Polishing may damage the multilayer coating by smearing the interface between coatings or inducing surface hardening. In order to determine whether polishing induced material property changes in any layer of the multilayer coating, a more rigorous investigation was undertaken. Witness coupons were formulated alongside the TPO/AP/BC/TC (bake and WOW processing) multilayer samples. These witness samples were TPO/AP and TPO/AP/BC. They were processed at the same time and conditions as those of the bake laminate samples. The coupons were used as received (unmounted) or mounted in epoxy and polished. The objective was to determine whether the surface modulus of an unmounted and unpolished coating layer was different from that of the mounted and polished multilayer coating.

The free surface of the unmounted coatings was indented to a depth of 2 μm using a 10 μm 90° conical tip (all coatings) and a 1 μm 60° conical tip (only the TPO/AP/BC/TC WOW samples). These measurements are named top down here. The average modulus was calculated in the depth range of 1−2 μm for the 10 μm 90° conical tip and 0.5−1 μm for the 1 μm 60° conical tip. Figure 5 shows a comparison of the top-down modulus to the modulus measured within the cross section. Note that the TC modulus in the cross-sectioned sample was the average modulus from 4 to 14 μm into the TC from the epoxy/TC interface; therefore, the standard deviation from this average is larger than that of the top-down indentation measurements. The agreement between the top-down and cross-sectioned moduli for the TPO/AP/BC/TC samples is excellent. This quantitative agreement supports the conclusion that the gradient in the TC modulus is not related to indentations near the mounting epoxy and that polishing did not significantly impact the modulus of the BC and TC coatings. Similarly, Figure 5 shows the top-down and cross-sectioned modulus comparison for two-layer TPO/AP samples. It was difficult to prepare a cross section of the two-layer TPO/AP witness coatings without the polishing process visibly damaging the AP layer. In light of these difficulties, a comparison was made between the

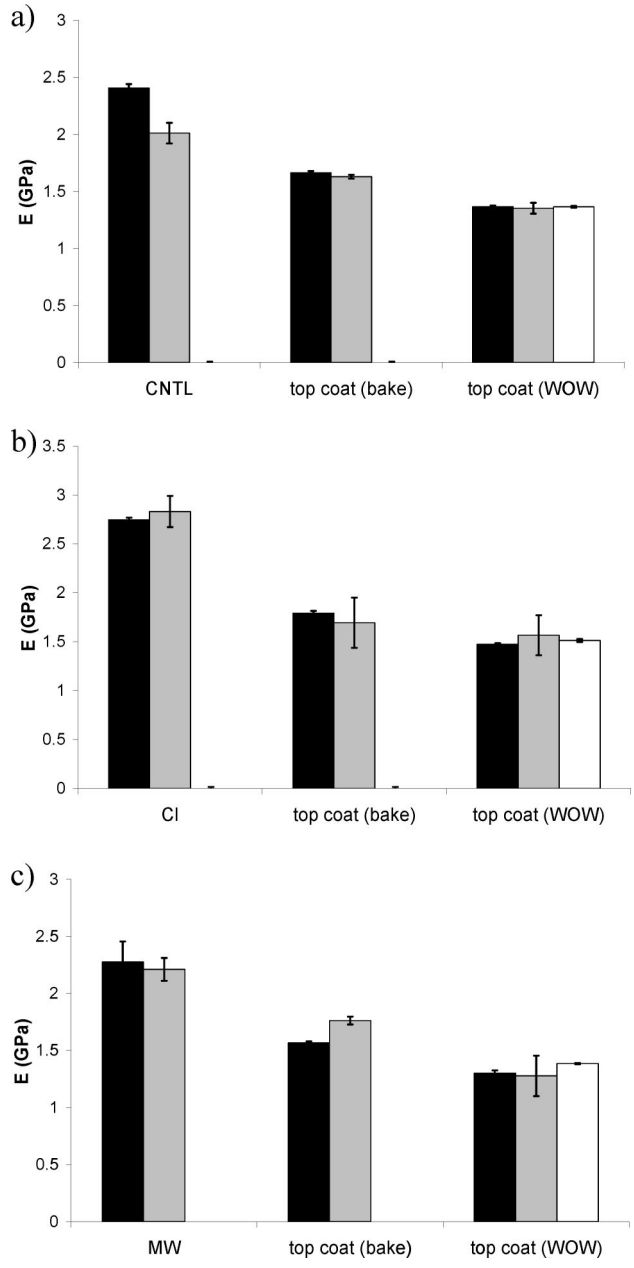

FIGURE 5. Comparison of the moduli measured on the polished, cross-sectioned, multilayer samples to the moduli measured on the unmounted witness samples (a) CNTL, (b) Cl, and (c) MW: (■) top-down measurement using a 10 μm 90° cone; (gray □) cross-sectioned measurement using a 1 μm 60° cone; (□) top-down measurement using a 1 μm 60° cone.

unmounted TPO/AP top-down modulus to the center of the AP section in the TPO/AP/BC/TC (bake processing) cross-sectioned samples. The agreement between the unmounted and epoxy-mounted polished cross-sectioned samples is excellent. The CNTL cross-sectioned modulus is slightly lower than the top-down measurement on that TPO/AP sample. CNTL is the same AP that exhibited a reduction in the modulus with WOW processing, and this may be an indication that the mechanical properties of this AP are more sensitive to the processing conditions or solvent. Raman measurements showed no spectroscopic indication of smearing of TPO into the AP layer or vice versa. Polishing

was not believed to have a significant impact on the mechanical properties of the other layers.

CONCLUSIONS

Different layers of a painted TPO panel were chemically and mechanically characterized as a function of the AP molecular weight, chlorine content, and processing method. The TC and BC chemistry and processing were kept constant along with the TPO type. Confocal Raman spectroscopy and DSI were used to characterize the samples. It was found that, within the lateral resolution of both instruments ($\approx$1 μm), the AP interface was sharp and independent of the structure and processing. This confirms the idea that the diffusion length scale of AP into the TPO, above several mass percent, is less than 1 μm. DSI measurements measured an increase in the modulus of the TC near the free surface of the coating. The CNTL AP was the only material that was sensitive to either processing or polishing. The cross-sectioned CNTL modulus processed using the WOW method was lower (1.66 $\pm$ 0.10 GPa) compared to the cross-sectioned CNTL modulus processed using the bake method (2.01 $\pm$ 0.01 GPa). The highest CNTL modulus (2.31 $\pm$ 0.03 GPa) was measured from top-down indentation measurements on CNTL/TPO bilayer coupons processed using the bake method. The modulus of the higher chlorine content or higher molecular weight AP did not change with the processing method. The TC and BC modulus was not affected by the AP type, processing, or sample polishing.

Acknowledgment. This work was conducted through the NIST/Industry Polymer Interface Consortium. The members of this consortium at the time that this research was conducted were Eastman Chemical, Visteon, Arkema Inc., Dow Chemical, and MTS. The authors thank Dr. Peter Drzal for development of the initial indentation measurements on these automotive coating systems. The authors thank Dr. Rose Ryntz (IAC Group), Dr. Lou Germinario (Eastman Chemical), and Dr. Erik Herbert (Agilent) for helpful discussions.

APPENDIX A

Definitions of Acronyms

TPO	thermoplastic polyolefin
AP	adhesion promoter
DSI	depth-sensing indentation
BC	base coat
TC	top coat
WOW	wet-on-wet processing
CNTL	control adhesion promoter
CL	higher chlorine content adhesion promoter
MW	higher molecular weight adhesion promoter

REFERENCES AND NOTES

(1) Ryntz, R. A. *JCT Res.* **2006**, *3*, 3–14.
(2) Burnett, D. J.; Thielmann, F.; Ryntz, R. A. *JCT Res.* **2007**, *4*, 211–215.
(3) Lawniczak, J. E.; Williams, K. A.; Germinario, L. T. *JCT Res.* **2005**, *2*, 399–405.
(4) Ryntz, R. A.; Xie, Q.; Ramamurthy, A. C. *J. Coat. Technol.* **1995**, *67*, 45–55.
(5) Ryntz, R. A. *Prog. Org. Coat.* **1996**, *27*, 241–254.
(6) Morris, H. R.; Munroe, B.; Ryntz, R. A.; Treado, P. J. *Langmuir* **1998**, *14*, 2426–2434.
(7) Morris, H. R.; Turner, J. F., II; Munroe, B.; Ryntz, R. A.; Treado, P. J. *Langmuir* **1999**, *15*, 2961–2972.
(8) Map, Y.; Winnik, M. A.; Yaneff, P. V.; Ryntz, R. A. *JCT Res.* **2005**, *2*, 407–416.
(9) Ryntz, R. A. *J. Vinyl Addit. Technol.* **1997**, *3*, 295–300.
(10) Clemens, R. J.; Batts, G. N.; Lawniczak, J. E.; Middleton, K. P.; Saas, C. *Prog. Org. Coat.* **1994**, *24*, 43–54.
(11) Waddington, S.; Briggs, D. *Polym. Commun.* **1991**, *32*, 506–508.
(12) Mirabella, F. M.; Dioh, N.; Zimba, C. G. *Polym. Eng. Sci.* **2000**, *40*, 2000–2006.
(13) Tang, H.; Martin, D. C. *J. Mater. Sci.* **2002**, *37*, 4783–4791.
(14) Ryntz, R. A.; Britz, D.; Mihora, D. M.; Pierce, R. *JCT Res.* **2001**, *73*, 107–115.
(15) Yin, Z.; Ma, Y.; Chen, W.; Coombs, N.; Winnik, M. A.; Ryntz, R. A.; Yaneff, P. V. *Polymer* **2005**, *46*, 11610–11623.
(16) Drzal, P. L.; Sung, L.-P.; Brintz, D.; Ryntz, R. A. *International Coatings for Plastics Symposium Proceedings*, June 6—8, 2005.
(17) Gu, X. H.; Michaels, C. A.; Drzal, P. L.; Jastnin, J.; Martin, D.; Nguyen, T.; Martin, J. W. *JCT Res.* **2007**, *4*, 389–399.
(18) Corle, T. R.; Kino, G. S. *Confocal Scanning Optical Microscopy and Related Imaging Systems*; Academic Press: New York, 1996.
(19) Fischer-Cripps, A. C. *Nanoindentation*; Springer-Verlag: New York, 2004.
(20) Sneddon, I. N. *Int. J. Eng. Sci.* **1965**, *3*, 47–57.
(21) Oliver, W. C.; Pharr, G. M. *J. Mater. Res.* **1992**, *7*, 1564–1583.
(22) Van Landingham, M. R. *J. Res. Natl. Inst. Stand. Technol.* **2003**, *108*, 249–265.
(23) White, C. C.; Van Landingham, M. R.; Drzal, P. L.; Chang, N.-K.; Chang, S.-H. *J. Polym. Sci., Part B: Polym. Phys.* **2005**, *43*, 1812–1824.
(24) Gu, X. H.; Michaels, C. A.; Nguyen, D.; Jean, Y. C.; Martin, J. W.; Nguyen, T. *Appl. Surf. Sci.* **2006**, *252*, 5168–5181.
(25) Adamsons, K. *Prog. Org. Coat.* **2002**, *45*, 69–81.
(26) Tadokoro, H.; Kobayashi, M.; Ukita, M.; Yasufuku, K.; Murahashi, S.; Torii, T. *J. Chem. Phys.* **1965**, 1432.
(27) Rosasco, G. L.; Blaha, J. J. *Appl. Spectrosc.* **1980**, *34*, 140–144.
(28) Ma, Y.; Farinha, J. P. S.; Winnik, M. A.; Yaneff, P. V.; Ryntz, R. A. *Macromolecules* **2004**, *37*, 6544–6552.
(29) Johnson, K. L. *Contact Mechanics*; Cambridge University Press: Cambridge, U.K., 1985.
(30) Hui, C. Y.; Jagota, A.; Lin, Y. Y.; Kramer, E. J. *Langmuir* **2002**, *18*, 1394–1407.
(31) Duskova-Smrckova, M.; Dusek, K. *J. Mater. Sci.* **2002**, *37*, 4727–4935.
(32) Flosbach, C. *Macromol. Symp.* **2002**, *187*, 503–513.

AM800152X